Structure, Vol. 12, 1087–1097, June, 2004, ©2004 Elsevier Ltd. All rights reserved. DOI 10.1016/j.str.2004.03.020

The Crystal Structure of the Carboxy-Terminal Dimerization Domain of htpG, the *Escherichia coli* Hsp90, Reveals a Potential Substrate Binding Site

Seth F. Harris, Andrew K. Shiau, and David A. Agard*
The Howard Hughes Medical Institute and
The Department of Biochemistry and Biophysics
University of California, San Francisco
San Francisco, California 94143

Summary

Hsp90 is a ubiquitous, well-conserved molecular chaperone involved in the folding and stabilization of diverse proteins. Beyond its capacity for general protein folding, Hsp90 influences a wide array of cellular signaling pathways that underlie key biological and disease processes. It has been proposed that Hsp90 functions as a molecular clamp, dimerizing through its carboxy-terminal domain and utilizing ATP binding and hydrolysis to drive large conformational changes including transient dimerization of the amino-terminal and middle domains. We have determined the 2.6 Å X-ray crystal structure of the carboxy-terminal domain of htpG, the *Escherichia coli* Hsp90. This structure reveals a novel fold and that dimerization is dependent upon the formation of a four-helix bundle. Remarkably, proximal to the helical dimerization motif, each monomer projects a short helix into solvent. The location, flexibility, and amphipathic character of this helix suggests that it may play a role in substrate binding and hence chaperone activity.

Introduction

The high abundance of Hsp90 in both eukaryotes and prokaryotes (0.5%–2% of cytosolic proteins) as well as extensive molecular genetic and biochemical studies indicate that members of the Hsp90 family play a role in general protein folding. However, in eukaryotes a discrete set of proteins has evolved a more specific dependence on Hsp90 for full function. A partial inventory of this growing group includes steroid hormone receptors, nitric oxide synthases, transcription factors, many kinases, telomerase, tubulin, and various viral proteins. Thus, Hsp90 is important for many basic cellular processes such as mitochondrial import (Young et al., 2003) and centrosome function (de Carcer et al., 2001), as well as cellular signaling events such as the assembly (Pratt and Toft, 1997) and disassembly (Freeman and Yamamoto, 2002) of transcriptionally active steroid receptor complexes. Indeed, consistent with its essential role in regulating signaling pathways, inhibition of Hsp90 activity can block cell proliferation. Such therapeutic utility is highlighted by the antitumor properties of the Hsp90 inhibitor, geldanamycin, a derivative of which (17-allylaminogeldanamycin) is being evaluated in human trials for efficacy against certain cancers (reviewed in Neckers, 2002). Variation in Hsp90 function has also been realized as a molecular mechanism underlying evolution (Rutherford and Lindquist, 1998; Queitsch et al., 2002). In sum, this ubiquitous chaperone impacts a wealth of processes over a huge range of both biological themes and time scales, influencing molecular events with fluctuations on the order of seconds while also helping to shape organisms over the passage of eons.

The ongoing discovery of the biological roles of Hsp90 has outpaced elucidation of the molecular mechanisms underlying its function. The protein contains three major domains (Figure 1): the amino-terminal domain (1_{1}-211_{216}) (numbering is *E. coli* htpG with human Hsp90β subscripts) which contains an ATP binding site, the middle domain (232_{287}-500_{553}), and the carboxy-terminal domain (502_{555}-624_{724}) which is required for homodimerization (Nemoto et al., 1995). Crystallographic studies of the isolated amino-terminal domains from the yeast and human proteins provided the first direct evidence that Hsp90 binds ATP and that Hsp90 inhibitors such as geldanamycin and radicicol compete with nucleotide for the same binding site (Prodromou et al., 1997; Stebbins et al., 1997). These structures also identified Hsp90 as a member of the GHKL (Gyrase, Hsp90, Kinase, MutL [reviewed in Dutta and Inouye, 2000]) family of proteins, whose nucleotide binding domains share a common architecture. Prior studies of the gyrase and MutL proteins indicated that the nucleotide binding domains of these enzymes dimerize in response to nucleotide binding. Subsequent analogous biochemical studies of Hsp90 revealed that ATP binding also promotes transient association of its amino-terminal domains, which in turn stimulates ATP hydrolysis (Prodromou et al., 2000; Richter et al., 2001). The requirement of transient dimerization for hydrolysis is further supported by the recent determination of the crystal structure of the middle domain from yeast Hsp90. Molecular modeling of the ATP-mediated dimer and mutagenesis experiments suggest that residues from the middle domains complete a domain-swapped active site (Meyer et al., 2003). Finally, recent structural and biochemical studies have defined the amino-terminal and middle domains as the binding sites for the cochaperones, p50(cdc37) and Aha1, respectively. These results suggest possible molecular mechanisms by which p50(cdc37) inhibits and Aha1 stimulates hsp90 ATPase activity (Meyer, 2004; Roe et al., 2004).

The Hsp90 carboxy-terminal domain contributes to chaperone function in several ways. As the interaction between the amino-terminal domains is relatively weak, their efficient contact, and thereby nucleotide hydrolysis, is dependent upon the carboxy-terminal dimerization to ensure high local concentration of the amino-terminal modules and their appropriate geometric disposition. Deletion of the carboxy-terminal domain abrogates ATP hydrolysis (Scheibel et al.,1998; Prodromou et al., 2000; Weikl et al., 2000; Wegele et al., 2003) and compromises yeast viability (Louvion et al., 1996). Additionally, the carboxy-terminal tail of eukaryotic Hsp90

*Correspondence: agard@msg.ucsf.edu

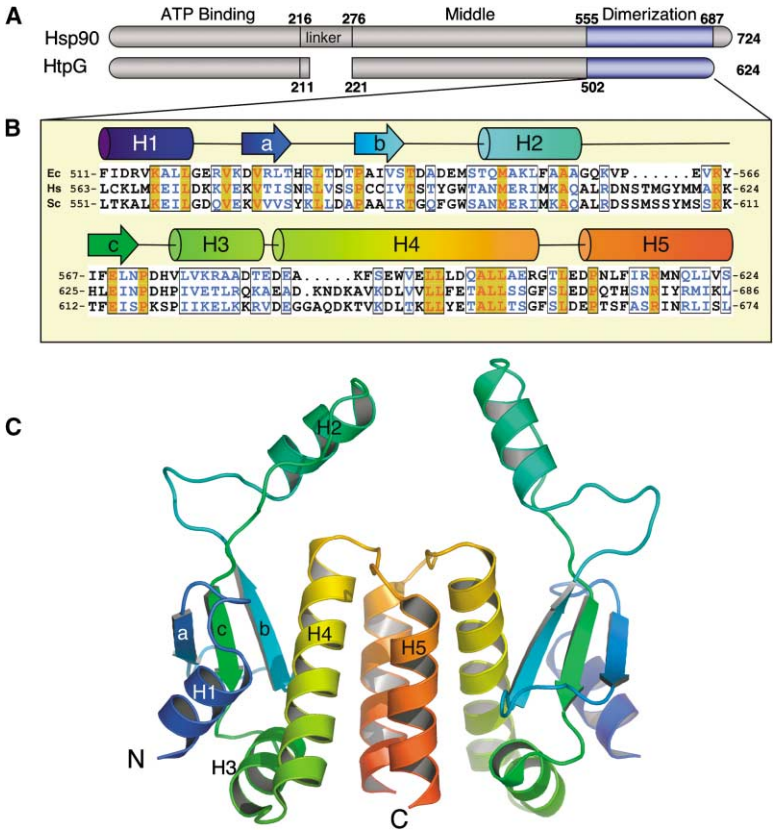

Figure 1. Sequence Alignment and Structure of htpG Carboxy-Terminal Domain

(A) Domain organization of Hsp90 proteins. Prokaryote homologs have a much shorter charged linker between amino-terminal and middle domains and lack an ~40 residue carboxy-terminal tail ending in MEEVD that is bound by TPR-domain cochaperones.

(B) Sequence alignment of *E. coli* htpG (Ec), human Hsp90β (Hs), and *S. cerevisiae* Hsp82 (Sc) with the secondary structure of the solved htpG fragment.

(C) Cartoon of the solved htpG dimer structure, color-coded to match the alignment above. Helices 4 and 5 create the majority of the dimer interface through a four-helix bundle, while helix 2 is in a remarkable exposed position on an extended loop.

provides the binding site for several Hsp90 cochaperones that influence ATP affinity or hydrolysis (e.g., Hop [Scheufler et al., 2000]) and some of these cofactors may also provide additional binding sites for protein substrates. The isolated carboxy-terminal domain is independently capable of stimulating protein folding as a passive chaperone (Shaknovich et al., 1992; Shue and Kohtz 1994; Young et al., 1997; Scheibel et al., 1998; Johnson et al., 2000). Finally, substrate binding could not be separated from dimerization activity in a small carboxy-terminal construct (Yamada et al., 2003).

Although the carboxy-terminal domain is critical for Hsp90 structure and function, high-resolution structural information has been lacking. Here we present the crystal structure of the carboxy-terminal domain of the *E. coli* Hsp90 homolog, high-temperature protein G (htpG). This structure reveals the mode of htpG dimerization, which occurs through the formation of a four-helix bundle, and that overall this domain possesses a previously unobserved fold. Furthermore, the domain presents a solvent-exposed, mobile, amphipathic helix that is likely to function as a protein substrate binding site. These data confirm and extend the importance of the carboxy-terminal domain in both Hsp90 ATPase and chaperone activities.

Results

Structure Solution

Based on limited proteolysis and sequence alignment information, numerous carboxy-terminal domain fragments of htpG were produced. Of these, a hexahistidine-tagged construct including htpG residues 511–624 (carboxy terminus) produced useful crystals. Initial crystals diffracted to only 3.5 Å and were in space group F222. Selenomethionine-substituted protein formed crystals similar in morphology, although these crystals were in space group P622 and contained a single monomer per crystallographic asymmetric unit. This crystal form was phased by multiwavelength anomalous dispersion (MAD) methods (Hendrickson, 1991), and the resulting partially interpretable maps allowed the construction of an incomplete model that nonetheless showed the major features of the domain. At lower pH and with longer incubation periods, a third crystal form containing eight copies per asymmetric unit in the space group $P4_32_12$ was grown. Both native and selenomethionine versions of the protein could be grown in this crystal form, which diffracted to 2.6 Å (Table 1). These data were phased using selenomethionine MAD, allowing calculation of a map of sufficient clarity that permitted tracing of all htpG residues present in the original construct, as well as a portion of the hexahistidine tag in three of the eight noncrystallographic copies. During refinement, strict noncrystallographic symmetry (NSC) restraints were used initially, then relaxed after the first two rounds of rebuilding, and ultimately removed. In addition, 486 solvent molecules, 3 nickel ions, and 3 chloride ions have been added to the model. After refinement, the final R and R_{free} were 22.7 and 26.6, respectively. The average rmsd from the mean between all eight copies when their backbone atoms are aligned is 0.97 Å (nonhydrogens) and 0.58 Å (backbone only).

Table 1. Statistics of Data Collection and Refinement

Data set	SeMet $P4_32_12$ a = b = 103.5 Å, c = 249.7 Å 90°, 90°, 90°			SeMet P622 a = b = 98.7, c = 107.0 90°, 90°, 120°	
Beamline	ALS 8.3.1			ALS 8.3.1	
Solvent	57% (8 mol/asu)			76% (1 mol/asu)	
Unique observations	76,375			11,628	
Wavelength Å (eV)	1.1271 (11000)	0.9792 (12662)	0.9790 (12664)	1.0781 (11500)	0.9795 (12653)
Resolution (Å)	2.6	2.8	2.8	3.5	3.5
Completeness (%)	96.3 (70.5)	99.9 (100.0)	99.7 (100.0)	99.6 (100.0)	99.1 (96.4)
Multiplicity	5.0 (2.5)	6.0 (5.9)	6.0 (5.9)	10.1 (8.8)	9.9 (8.0)
R_{sym}[a]	0.063 (0.62)	0.094 (0.75)	0.096 (0.78)	0.117 (0.605)	0.095 (0.369)
$I/\sigma I$	19.5 (1.5)	18.0 (2.7)	17.6 (2.6)	16.6 (2.63)	19.8 (3.4)
Phasing ($P4_32_12$ form)					
Sites	24				
FOM (after density modification)	0.5972 (0.8976)				
Refinement ($P4_32_12$ form)					
Resolution range (Å)	30–2.6				
Protein atoms	7416				
Ion atoms	3 Cl, 3 Ni				
Solvent atoms	486				
R_{cryst}/R_{free}[b]	22.7/26.6				
Mean B	60.3				
Rmsd bond lengths (Å)	0.008				
Rmsd bond angles (°)	1.2				

Parentheses denote statistics for highest resolution bin.
[a] R_{sym} = sum(|I − <I>|)/sum(I); I is intensity.
[b] R = sum($|F_{obs} - F_{calc}|$)/sum(F_{obs}); F_{obs}, observed structure-factor amplitude; F_{calc}, calculated structure-factor amplitude.

Fold Description

The carboxy-terminal domain's fold starts with a short α helix (H1) leading to a small three-stranded antiparallel β sheet (strands a, c, and b). An extended, exposed loop between strands b and c contains a second short helix (H2). The β sheet is followed by helices H3, H4, and H5 with the last two longer helices forming the bulk of the dimerization interface (Figures 1 and 2). Structural comparisons performed using DALI did not yield any high scoring results (top Z score was 3.1 where scores less than 2.0 are considered structurally dissimilar) (Holm and Sander, 1993). The closest match, a metalloendopeptidase (PDB code 1GE5), did show limited similarity in the framework of a small β sheet and two helices that have a geometric arrangement akin to the β sheet and helices H1 and H3 in the htpG carboxy-terminal domain. However, the remaining elements of the architectures of these proteins are essentially unrelated.

The Dimerization Motif

In both crystal forms, the two long carboxy-terminal helices (H4 and H5) interact with their equivalent counterparts from a second molecule around 2-fold symmetry axes (both crystallographic and noncrystallographic examples are present in the crystals) to form the dimer via a four-helix bundle (Figure 2). The helices follow an up-down-up-down topology with an angle of −130° between the helices within each monomer and an antiparallel juxtaposition of H5 of one monomer and H4′ of the partner monomer (−178°). The geometry of these dimer interface elements is quite constant across all the NCS copies and multiple crystal forms solved. These interhelical angles are relatively common for general helix-helix crossings, with 50° (quasi equivalent to −130°) representing "classical" ridge-into-groove packing between *i*+*4* layers (Chothia, 1984). Using the htpG four-helix bundle as a search target, we discovered considerable similarity with myohemerythrin (DALI Z score = 6 [Holm and Sander, 1993]) and cytochrome c′ (Z score = 5.9), though these had more moderate packing angles or an alternate overall bundle topology, respectively. Among lower scoring matches, CheA (Z score = 4.4) is notable as this histidine kinase is a bacterial signaling protein that is also a member of the GHKL superfamily, thus sharing structural similarity to Hsp90 in its ATP binding domain as well.

The HtpG interface buries ~930 Å^2 surface area per monomer. Common to many four-helix bundles, the buried surface is predominantly hydrophobic (Figure 3) and fringed by a few charged residues. Helix 5 is embraced in a hydrophobic groove formed by helices 3′, 4′, and 5′ on the partner monomer. The panels of Figure 2B show this packing arrangement at successive cross-sections through these helices. Trp592, Leu621, and Leu622 form extensive nonpolar contacts with their dimeric counterparts at the base level. On the next layer up, the hydrophobic contacts formed by Met618 with its dimeric partner are flanked by two sets of hydrogen bonds between the side chains of Asn619 and Gln599 from the other monomer. Finally, Phe614 extensively contacts its dimeric partner at the top level. Leu602 and Pro611 on the terminal turns of helices 4 and 5, respectively, flank Leu608, which projects down from the interhelix loop to provide an arched hydrophobic "ceiling" to the dimer interface. The outer surface of this loop is composed of the polar residues Arg605, Thr607,

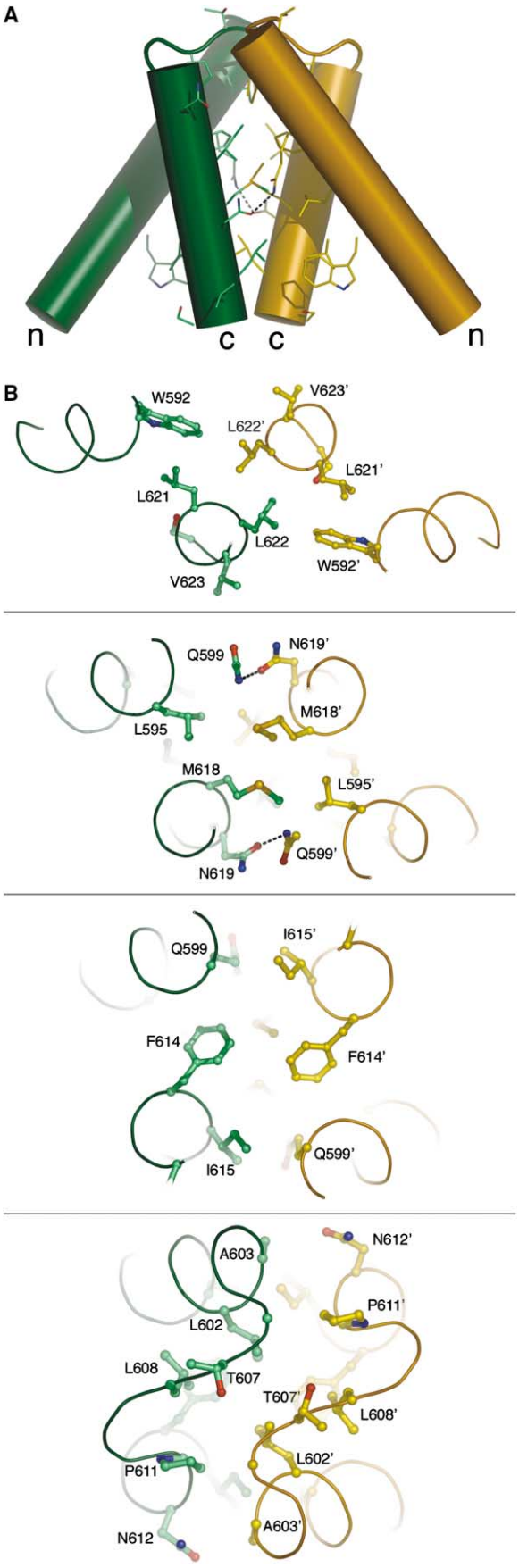

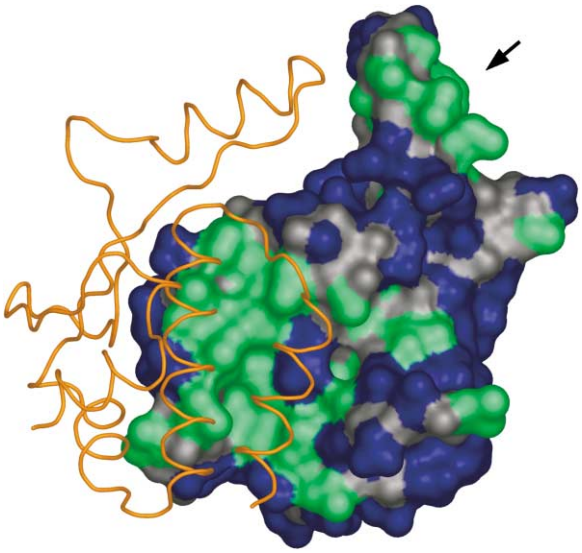

Figure 3. Hydrophobic Exposure in the Dimer Interface and on Helix 2

The htpG dimer with one monomer in surface representation showing the long hydrophobic groove that embraces the final helix of the partner monomer (orange). The surface is colored such that hydrophobic side chains are green, polar side chains are blue, and backbone atoms are gray. This delineates a large hydrophobic patch over the dimer interface and a lesser one on the exposed back of helix 2 (arrow).

Glu609, and Asp610, which project their side chains into solvent. Strictly speaking, the dimer interface is not purely composed of residues of the four-helix bundle, as Val575 and Leu576 on helix 3 form hydrophobic contacts alongside Trp592 with Val623′. The loop residues Asp534, Thr535, and Pro536 are also proximal to the Gln599:Asn619′ hydrogen bond and extend the contact groove for the partner monomer's helix 5′.

Strong sequence conservation that maps to the surface is clustered in the dimer interface and extends onto a portion of the exposed helix 2 (Figure 1B). Along the dimer interface, several hydrophobic residues are among the most conserved (Leu602, Leu576, Pro611, Phe614) followed closely by the polar residues Asn619 and Gln599. Beyond these conserved residues, there is variability between Hsp90 homologs in the identity of the hydrophobic residues that constitute the remainder of the dimerization surface. These sequence differences (and hence differences in shape complementarity) likely underlie the heterodimerization specificity patterns observed for Hsp90 homologs (Nemoto et al., 1996; Garnier et al., 2001).

Figure 2. The Four-Helix Bundle Dimer Interface

(A) Helix packing geometry of the up-down-up-down bundle. Intramonomer helix angles are −130° and intermonomer angles are −178° (Walther, 1997).

(B) Cross-sections of successive layers of the dimer interface. Only side chains on the helices whose accessibility changes upon dimerization are shown in stick representation. The core shows a preponderance of hydrophobic residues (Leu, Phe, and Met) flanked by a few polar interactions (e.g., the intermonomer hydrogen bond between Q599 and N619′).

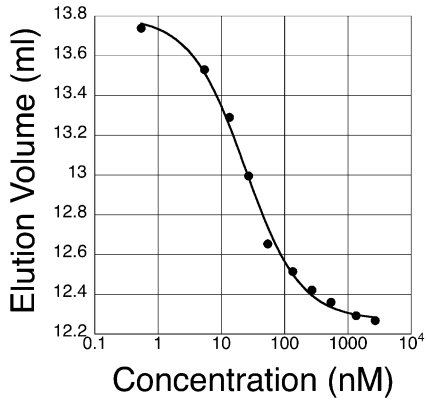

Figure 4. Determination of the htpG Dimer K_d

The plot shows mobility of full-length htpG on a size exclusion chromatography matrix versus protein concentration at the point of elution. Higher concentration injections show an elution point consistent with a dimer while the lowest detectable concentrations approach the monomer elution point. Intermediate positions reflect the equilibrium between monomer and dimer that is rapid relative to the time scale of the chromatography. The midpoint gives a measure of the dimerization K_d, which when corrected for dilution during the column run (16.6-fold based on peak height) is ~24 nM.

htpG Dimer Dissociation Constant

We have determined the dissociation constant of the htpG dimer, applying a similar size exclusion chromatography method as used for yeast Hsp82 (Richter et al., 2001). Fitting a two-state equilibrium model to a plot of elution time versus protein concentration and correcting for dilution effects gives a K_d of ~24 nM for full-length htpG (Figure 4) which compares well with the 60 nM value found for yeast Hsp82 (Richter et al., 2001). Reduced absorbance limited our ability to determine an accurate value for the carboxy-terminal dimerization fragment alone, but it appeared to have a K_d at least 25-fold weaker than that for full-length htpG. Experiments with the yeast protein indicated that a long carboxy-terminal fragment (residues 262–709) had a dimerization affinity (45 nM) near to that of full-length Hsp82, although the K_d of a shorter fragment (527–709) closer in size to our high-K_d htpG construct could not be measured for comparison (Richter et al., 2001).

Helix 2 is Amphipathic, Exposed, and Mobile

An unexpected feature of our structure was the projection of helix 2 away from the body of each monomer (Figure 1). Based on its conformation in the high-resolution structure, helix 2 and the contiguous loop do not appear to be required for the proper folding of the remainder of the domain. The density for helix 2 is unambiguous in each of the eight NCS copies (Figure 5B), but superposition of the backbones of these chains shows it to be the most variably positioned region of the protein (rmsd from the mean for residues 544–565 is 0.94 Å for backbone atoms, 1.48 Å including side chains). A hydrophobic face of the helix is formed by Met546, Met550, Ala551, Leu 553, Phe554, and Ala556, and intriguingly, this is exposed to solvent. Although the identities of the hydrophobic residues from helix 2 (with the exception of Met550) are modestly variable among the different Hsp90 homologs, the hydrophobic character of this helical face is absolutely conserved across species. Methionines in particular are abundant in this region in all homologs. Eukaryotic Hsp90s tend to have approximately six extra residues after the helix, two of which (or even three in Hsp90β) are also methionines (Figure 1). Thus, the Hsp90 dimer would have a cluster of eight to ten methionines in a relatively localized region where two of these helices are situated.

Crystal contacts in both the P622 and the higher resolution $P4_32_12$ crystal forms suggest that helix 2 has the propensity to mediate protein:protein interactions. In the latter case, the molecules are organized in the asymmetric unit in two tetramers, with helix 2 from each monomer meeting at a central four-way node (Figure 5C). As mentioned above, two methionines are placed in this vicinity by each molecule, so the juxtaposition of these four chains creates an array of eight methionines in a small box bounded by the four helices (Figure 5D). The diverse contacts made by helix 2 of the different monomers demonstrate its plasticity as an interaction surface. Another mode of interaction is suggested by the lower resolution crystal data we first obtained. Initial phasing of the 3.5 Å P622 crystal data relied on a single well-ordered (seleno)methionine site at the dimer interface; the two methionine positions of helix 2 were not apparent. Curiously, the crystal thus appeared formed of widely spaced layers of protein with no apparent contacts between strata. This seemingly impossible crystal packing arrangement is explained by superimposition of the higher resolution structure on the partial P622 model, whereby helix 2 is positioned between the crystal layers. Helix 2, therefore, is likely mediating the necessary protein:protein interactions, in this case around a crystallographic 3-fold axis. While we have not refined the model for this crystal form, the approximate position of helix 2 in these distinct environments clearly suggests additional modes of helix 2 interaction.

Discussion

As the carboxy-terminal region of Hsp90 is critical for its full function, it is essential to understand the details of this domain and elaborate potential means of its regulation. We have determined that the htpG carboxy terminus dimerizes using a four-helix bundle motif centered on a 2-fold symmetry axis. The htpG dimer affinity of 24 nM is close to the 60 nM value measured for yeast Hsp82 (Richter et al., 2001), while dimerization of the isolated carboxy-terminal fragment appears to be less strong. This indicates that other parts of the protein, (i.e., the middle and amino-terminal domains) contribute to dimerization.

Eukaryotic Hsp90s have a small carboxy-terminal extension that provides a binding site for TPR-containing cofactors that is not present in the prokaryotic htpG. The last residue of htpG at position 624 does, however, indicate the departure point for the additional ~40 amino acid tail which contains the MEEVD sequence required for TPR recognition (Young et al., 1998). Notably, this site is on the opposite side of the molecule from the helix 2 projections (Figure 1). Even in the context of the

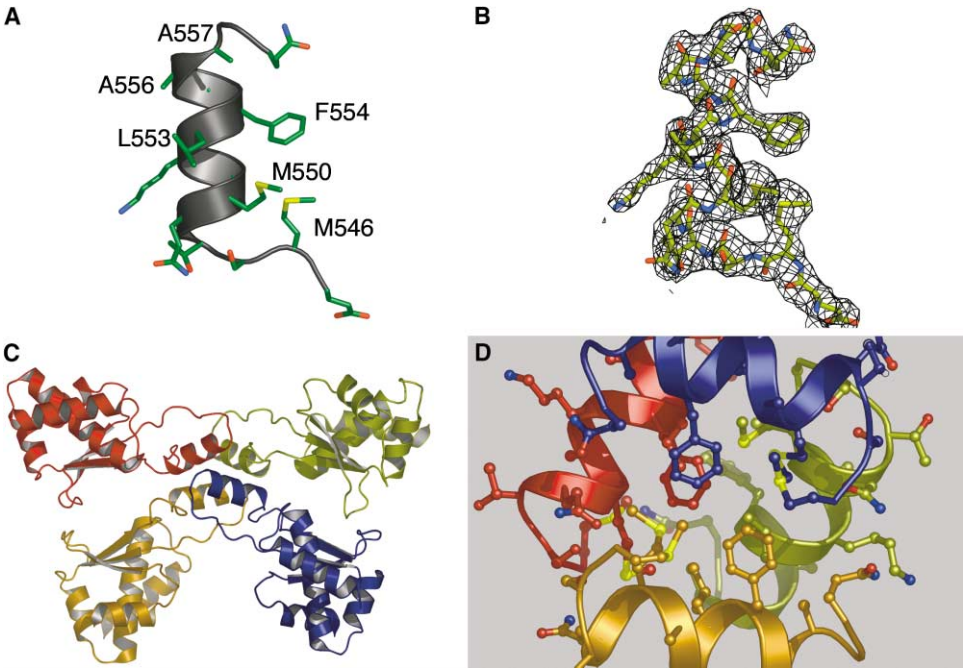

Figure 5. Description of the Extended Helix 2 Loop

(A) A cartoon of helix 2 showing a broad stripe of hydrophobic side chains, Met546, Met550, Leu553, Phe554, Ala556, and Ala557.

(B) A $2F_o$-F_c map shows good quality electron density for this feature even though it is the most variably positioned element between the eight NCS copies.

(C) Cartoon diagram representing one-half of the $P4_32_12$ crystal's asymmetric unit (asu), a layer of four monomers related by NCS. To complete the asu, a second similar layer lies rotated on top of this one, contacting the dimerization interfaces of the red and blue monomers that face up out of the page in this depiction. The gold and olive monomers would form their respective dimer contacts down into the page. Helix 2 loops from each monomer meet at a central four-way node.

(D) A cut-away view of the helix 2 packing at the four-way junction. An hydrophobic core is created by two arrays of four methionines (Met546, Met550) and four copies of Phe554. Polar residues forming the perimeter of the cluster are exposed to solvent.

crystal packing, this is a very accessible position, free and clear for interaction and displaying relatively limited residue conservation. Because the tethering point is at the seam of the dimer, it is well positioned for influencing Hsp90 oligomeric state, while being near to potential substrates and at the same time remaining clear of the Hsp90 dimer clamp.

Carboxy-Terminal Domain Mutations Underline Its Functional Importance

Several genetic and biochemical studies highlight the functional importance of the carboxy-terminal region itself. Deletion of the domain compromised yeast viability (Louvion et al., 1996), although some monomer species were noted to persist in interactions with estrogen receptor in vivo (Meng et al., 1996). Mutation of conserved leucine pairs to serines in Hsp90α's carboxy terminus (htpG equivalent positions 595, 596, 601, and 602) abrogated the ability of Hsp90α to prevent heat-induced aggregation of citrate synthase (Yamada et al., 2003). Deletion of residues 661–677 from chicken Hsp90 corresponding to parts of helices H4 and H5 (htpG 598-614), showed diminished binding to progesterone receptor (Sullivan and Toft, 1993). A slightly larger region of murine Hsp90 (643-690) was found to be necessary and sufficient for restoration of DNA binding activity of inactivated MyoD/E12 bHLH proteins (Shue and Kohtz, 1994). An overlapping stretch, which is predominantly buried upon dimerization, has been identified as the epitope for a unique Hsp90 antibody, AC88, that binds the free but not the substrate bound chaperone (Riehl et al., 1985; Chen et al., 1997). These studies describe a correlation between dimerization and substrate binding. However, in the absence of structural data it has been difficult to determine whether these carboxy-terminal regions are directly involved in physiologically relevant ligand contact (in addition to dimerization) or whether dimerization is indirectly required for more remote regions to be effective in substrate binding. Our structure, showing the extent of the dimer interface, indicates that for the bulk of these studies the latter is the simpler explanation for these data.

Residues in the dimer interface overlapping with the AC88 antibody epitope have also been identified as important for a putative second nucleotide binding site (Csermely and Kahn, 1991; Marcu et al., 2000; Owen et al., 2002; Soti et al., 2002). We do not observe any compelling feature that would account for this function, and again note that much of this epitope's surface is in fact buried upon dimer formation. Interestingly, however, this site is thought to bind nucleotide only when the primary amino-terminal site has bound ATP (Soti et al., 2002). This latter event stimulates association of the amino-terminal domains most likely in the manner used

by the nucleotide binding domains in the structurally homologous GHKL family members gyrase and MutL (Ban et al., 1999; Kampranis et al., 1999). Such a tether between amino-terminal domains could permit or even trigger conformational changes in the carboxy-terminal domains, including possible transient separation of the carboxy-terminal dimerization surfaces themselves. This exposure might unveil a cryptic secondary site, with interesting implications for the several studies described above that also implicate these residues in substrate binding. Validation of this hypothesis, however, will clearly require additional structural and functional studies.

The Exposed Helix 2 Has Properties Consistent with a Role in Substrate Binding

Accessibility, flexibility, and hydrophobicity are hallmarks of chaperone substrate binding sites, and our work identifies the striking helix 2 as bearing these traits. We recognize that Hsp90 will use diverse surfaces and modes for binding client proteins (e.g., it is capable of binding both Akt and eNOS substrates simultaneously [Fontana et al., 2002]), but the character of helix 2 combined with its particular location within the jaws of the htpG dimer (see below) strongly suggests this feature as one element used in substrate protein contact. The accessibility of this region is emphasized by its proteolytic sensitivity; we have identified htpG residue 560 as being a trypsin-sensitive site in the context of the full protein (data not shown), corroborating data from other studies (Hartson et al., 1999; Nemoto et al., 2001; Owen et al., 2002). Addition of molybdate, known to stabilize various Hsp90-substrate complexes, resulted in specific protection of this region of human Hsp90 from proteolysis, again providing biochemical evidence for the conformational flexibility of this feature (Hartson et al., 1999). The crystal packing interactions we observe exemplify the propensity of helix 2 to establish protein:protein contacts, noting the particular suitability of the several methionines to accommodate diverse hydrophobic geometries, as expected of partially denatured substrates. Indeed, these conformationally pliable hydrophobic side chains echo at a finer level those same characteristics of the chaperone as a whole.

Data from two prior studies support these ideas, attesting to the functional importance of helix 2 in particular. One carboxy-terminal deletion study tested removal of yeast Hsp82 residues 582–601 (corresponding to htpG 543-560 which encompasses 548–557 of helix 2), and this alone was sufficient to prevent viability (Louvion et al., 1996). Even more specifically, of several temperature-sensitive mutations found throughout yeast Hsp82 in a genetic screen, only one (A587T), corresponding to htpG position 548, had impaired ability to potentiate the exogenously supplied Hsp90 client, glucocorticoid receptor (GR), while still maintaining a wild-type doubling time at 25°C (Nathan and Lindquist, 1995). Tellingly, this substitution, whose unique phenotype is specific to a particular client, is at the base of helix 2.

The disposition of helix 2 within the context of the structure of full-length htpG lends further support to the role of this helix as a potential substrate binding site. The molecular envelope that we present in Figure 6 is based on a medium-resolution, partially interpretable density map for the full-length htpG (A.K.S., unpublished data). As such, we use it here only to interpret the large-scale, salient features of the protein. In particular, we were able to position the high-resolution structure of the carboxy-terminal domain into the full-length experimental map using its clear density for the four helices of the dimerization interface. Based on this docking, helix 2 from each monomer is located at the bottom of the canyon formed by the dimer walls. The large cleft appears an inviting and logical location for substrate binding, as it could thus provide maximum coverage and protection from aggregation.

The binding and release of partially folded substrates that are necessary for chaperone function require the chaperone to conditionally expose or conceal its hydrophobic binding sites. Such interplay of flexibility and hydrophobicity is exemplified by the GroEL/GroES chaperonin and in particular the motions of the GroEL apical domain during the folding cycle (for review see Bukau and Horwich, 1998). Regions of the apical domain required for substrate binding are noted for their higher B factors and conformational variability (Braig et al., 1995). These inherently malleable, multivalent hydrophobic patches that contact substrates explain the promiscuous but tight binding capability of the chaperonin (Chen and Sigler, 1999). Dynamic masking of the GroEL binding sites is stimulated by GroES, which competes with substrates for contacts with the same GroEL residues. The hydrophobic regions shift away from the accessible walls of the core volume in order to bind GroES. Addition of the GroES ring thus encloses the substrate while simultaneously achieving its release into the chaperonin cavity. Although it is topologically dissimilar to the GroEL apical domain, htpG's helix 2 does exhibit analogous physical properties. It combines plasticity (providing potential both to adapt to diverse substrates and to move to a nonbinding or masked conformation) and hydrophobic exposure with a logical position for substrate contact. Our structural work suggests several ways in which Hsp90's hydrophobic surfaces could be masked, and we have incorporated these in framing hypothetical models (Figure 7).

Models for Hsp90 Domain Movements during Substrate Binding and Release

We posit that helix 2 acts as one of several mobile, hydrophobic, protein binding surfaces in the jaws of the Hsp90 dimer. Meyer et al. recently identified an amphipathic mobile loop protruding from the middle domain (yeast Hsp82 327-340) proximal to residues important for binding the client protein PKB/Akt (Sato et al., 2000). Integrity of the adjacent, exposed W300 (htpG F257) was also important for activation of the Hsp90 client v-Src (Meyer et al., 2003, 2004). The alternate exposure and masking of multiple hydrophobic patches would need to be coupled to the binding and hydrolysis of ATP to relate this to substrate binding. In the full-length dimer, helix 2 of the carboxy-terminal domain comes within 7–10 Å of distal middle and amino-terminal domain elements of the partner monomer, including the hydropho-

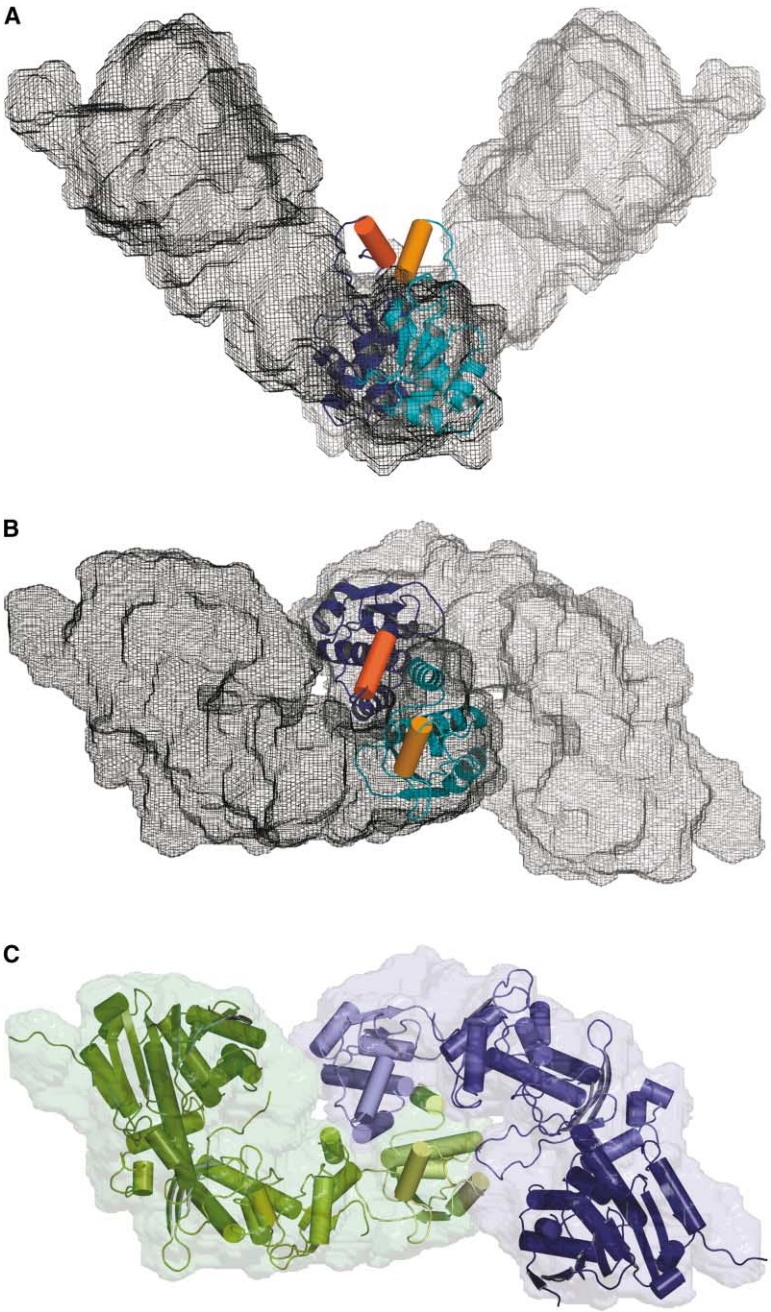

Figure 6. The Molecular Envelope of the Full htpG Dimer

Details of the full-length htpG structure are in preparation. The mask presented here was generated (MAMA [Kleywegt and Jones, 1999]) from an unrefined model of the intact htpG dimer (excluding the helix 2 region whose density is unclear in the full-length protein map). The higher resolution carboxy-terminal domain structure was aligned using the experimental maps as a guide. The resulting position of the carboxy-terminal domain shows the protrusion of helix 2 into the cleft of the dimer. The overall morphology shows an intimately wrapped dimer with relatively close approach between sequentially disparate domains of the two monomers.

(A) Side view. Helix 2 of each monomer is highlighted in red and orange.

(B) Top view, rotated 90° around the *x* axis relative to (A), displaying the marked curl of the dimer.

(C) Same orientation as (B). Manual docking of published amino-terminal and middle domain structures into the envelope (translucent surfaces) to create a composite full-length protein model. Within each monomer (one blue, one green) the amino-terminal domains (from PDB 1AMW) are in the darker shades, the middle domains (1HK7) in a medium shade, and the carboxy-terminal domains in the lighter shades at the center of the dimer.

bic loop from the middle domain that is intimated to be involved in protein binding for PKB/Akt. Given Hsp90's flexibility, this arrangement could provide routes to inter-domain (and intermonomer) communication.

There are several possible routes for substrate release: perhaps the simplest is reversal of the first step shown in Figure 7 with Hsp90's amino-terminal domains returning to the original separated state with the clamp open and once again poised for binding. Study of the intertwined dimer morphology (Figure 6) suggests a second option, as space in the Hsp90 cavity will be significantly restricted as the dimer clamp closes. Such steric restraints may mean that Hsp90 maintains substrate contact via only a small subdomain or extended piece of the substrate (Figure 7, middle frame). Taken further, mutual masking of helix 2 and the other hydrophobic binding surfaces may completely exclude the substrate, in which case closure of the Hsp90 dimer would constitute a mechanism for substrate release (Figure 7, top of last frame).

A third and more speculative possibility involves transient dissociation of the dimerization interface, while dimer integrity is preserved by amino-terminal domain contacts. A precedent for such dual-hinged motions exists in the topoisomerase II family, which are also members of the GHKL protein group (Berger et al., 1996). The interfaces that form the "second" gate of topoisomerase II (1150 Å^2) (PDB code 1BJT) and the prokaryotic

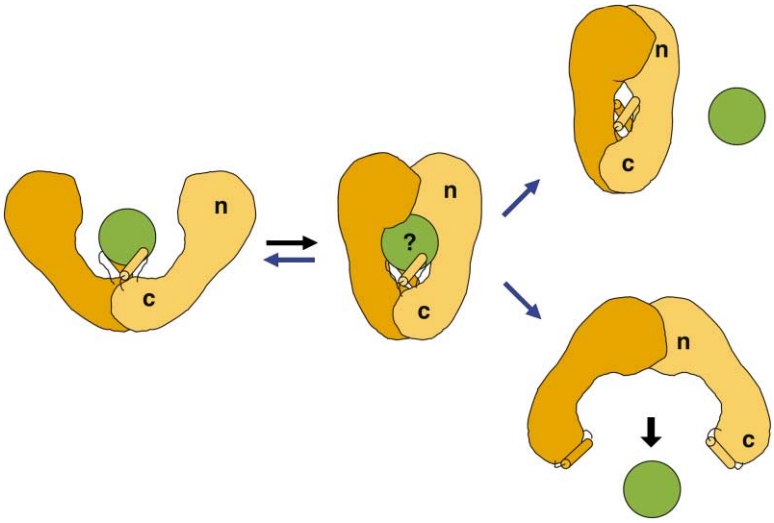

Figure 7. A Simplified Schematic of Possible Hsp90 Function

Substrate is represented as a green circle to mark the expected position of contacts, but not as a direct indication of substrate size or structural details. The bulk of the substrate may, in fact, be variously extended outside of the Hsp90 clamp with chaperone:substrate contacts limited to a subdomain or smaller structural element of the client protein. Also, binding of ATP is known to stimulate the association of the amino-terminal domains, but as the timing of hydrolysis and release is not yet well understood, these details have been excluded from these figures for simplicity. Substrate is presumed to bind within the Hsp90 dimer clamp, contacting multiple mobile hydrophobic elements including helix 2 of the carboxy-terminal domains (shown as cylinders) and loops or patches along the inner surface of the middle domain (not explicitly shown). The association of the amino-terminal domains, stimulated by ATP binding, occludes the inner volume and juxtaposes the hydrophobic features. We show three possible routes of substrate release (blue arrows). Reversal of the initial binding event may return the chaperone to its open state with amino terminal domains separated (left). Alternately, full closure of the clamp may be incompatible with substrate binding as the hydrophobic features are mutually masked (upper right). Finally, inspired by the GHKL family member topoisomerases, transient dissociation of the carboxy-terminal domains could cause the exposed hydrophobic dimer interface to compete for binding with helix 2, thereby synchronizing substrate release with an opening of the Hsp90 topological ring to permit substrate to exit the Hsp90 clamp (lower right).

GyrA (1090 Å^2) (1AB4) proteins are slightly larger than that formed in the htpG dimer (930 Å^2) and estimated to result in tighter binding, yet much evidence supports their opening to allow DNA strand passage. Therefore, the size and strength of the htpG dimer contact would not itself rule out the parting of the chaperone's carboxy-terminal interface. The flexibility of helix 2 prompts us to wonder whether, properly positioned, the helix 2 sequence 554-FLxxMQ-549 could mimic a significant portion of the contacts "normally" provided by helix 5 of the other monomer (614-FIxxMN-619) and thereby mitigate the exposure of the hydrophobic dimer interface during this hypothetical transient dissociation. The helix 2 tether is sufficient to achieve this configuration in htpG without significant rearrangements of existing secondary structure elements, and these motions are even more accessible in eukaryotic homologs due to the additional 6 amino acid insertion present in the flanking chain (Figure 1 sequence alignment). In the context of the dimer, this duality of helix 2 function nicely synchronizes the opening of a "back door" for substrate exit from the Hsp90 clamp with the release of the substrate from helix 2 as it turns to a masked position (Figure 7, bottom).

While this notion of helix 2's movement would also explain the correlation between dimerization and substrate binding (as any monomer would be expected to have helix 2 masking the dimerization interface and hence be unavailable for substrate binding), the model ignores, for example, the possibly potent influence of Hsp90 cofactors. Ongoing experiments will help determine if Hsp90 truly avails itself of the two-gate model pioneered by the GHKL-family member topoisomerases and whether helix 2 acts to regulate substrate binding as we have elaborated, or as a more simple brace between the dimer partners. The carboxy-terminal domain architecture described here provides the final missing piece in Hsp90 family structures, conferring important spatial restraints on the development of functional models. As the anchor point for the dimer, it directs the fundamental shape of this complex molecule.

Experimental Procedures

Protein Constructs

PCR was used to amplify a DNA fragment encompassing the coding region for residues 511–624 of *E. coli* htpG. The primers included restriction sites BamHI and HindIII which were used to insert the fragment into vector pQE80 (Qiagen).

Protein Purification

Protein was purified from induced *E. coli* cultures using Ni-NTA affinity resin for the 6×His tag, followed by anion exchange and size exclusion chromatography on a Superdex S200 column (Pharmacia). Protein was concentrated and exchanged into 20 mM Tris (pH 7.5) using Ultrafree Biomax concentrators (Millipore) to a final concentration of 40–60 mg/ml based on UV280 absorption. Protein was flash frozen in liquid nitrogen and stored at −80°C until use.

Crystallization

Large hexagonal protein crystal plates diffracting to 3.5 Å were grown by hanging drop vapor diffusion equilibrated against a well containing 0.8 M sodium malonate, 0.1 M Tris (pH 8) with and without various detergents. Rods of square cross-section were grown under similar conditions, but generally at lower pH (0.1 M sodium cacodylate, pH 6.5) and higher salt (1.3 M sodium malonate) and over longer incubations of up to 1 month. These rod crystals diffracted to 2.6 Å.

Full-Length htpG

The full details and description of the intact htpG structure are in preparation. In brief, native data from full-length wild-type htpG crystals were measured to ~4 Å. The phases derived from heavy atom information were improved by a combination of noncrystallographic and multicrystal form averaging using sharpened amplitudes. The resulting maps allowed the location of the amino-terminal and middle domains as well as the dimerization helices of the carboxy-terminal domain. These helices recapitulate the dimer interface observed in the isolated carboxy-terminal domain structure,

allowing its accurate positioning within the full-length protein experimental maps.

Data Collection, Processing, and Software

Data was collected at ALS beamline 8.3.1 at three wavelengths. Data reduction was accomplished using both DENZO (Otwinowski and Minor, 1997) and the ELVES suite (Holton and Alber, 2004) to manage the workflow from MOSFLM (Leslie, 1992) to other CCP4 utilities (CCP4, 1994) and ultimately SOLVE (Terwilliger and Berendzen, 1999). Phases were also calculated with CNS (Brunger et al., 1998) that located 20 of the 24 possible selenium sites. The other 4 sites were added manually and inspection of anomalous difference maps signified the presence of three additional peaks in the asymmetric unit that were interpreted as nickel ions which would be expected to show anomalous differences at these wavelengths. Also, portions of density from the amino terminus that appeared to be a segment of the 6×His tag of the construct was apparent and positioned to help chelate the nickel ion sites of two symmetry mates. Refinement was accomplished with CNS (Brunger et al., 1998) and manual rebuilding using O (Jones et al., 1991). Molecular graphics images were created using PyMOL (DeLano, 2002).

Size Exclusion Chromatography and Dimerization K_d

The determination of the dimer dissociation constant, K_d, was achieved following a method similar to Richter et al. (2001). In brief, htpG protein was run on a Superdex200 10/30 column in 100 μl injections at concentrations ranging from 70 μM down to 14 nM. Elution times were obtained from peak positions by monitoring absorbance at 280 and 215 nm for greater sensitivity. A curve was fit to the plot of concentration versus elution time (ET) satisfying the equation below:

$$ET = ET_{monomer} - (ET_{monomer} - ET_{dimer})\,[protein]/([protein] + K_d).$$

The resulting apparent K_d was adjusted by a factor to reflect the dilution of the sample during progression through the column. We assumed the monomer and dimer species were in equilibrium throughout the experiment, and the single peak observed in all traces suggests that this exchange was rapid in relation to the time course of the column run.

Acknowledgments

Funding for this project was provided by the Howard Hughes Medical Institute and NIH grant DK58390. S.F.H. was supported by a Helen Hay Whitney Foundation Fellowship. We wish to thank James Holton at the Advanced Light Source for support during data collection and Luke Rice for helpful discussion and comments. Coordinates for the PDB deposition 1HK7 were kindly provided by request from L. Pearl.

Received: February 5, 2004
Revised: March 17, 2004
Accepted: March 21, 2004
Published: June 8, 2004

References

Ban, C., Junop, M., and Yang, W. (1999). Transformation of MutL by ATP binding and hydrolysis: a switch in DNA mismatch repair. Cell *97*, 85–97.

Berger, J.M., Gamblin, S.J., Harrison, S.C., and Wang, J.C. (1996). Structure and mechanism of DNA topoisomerase II. Nature *379*, 225–232.

Braig, K., Adams, P.D., and Brunger, A.T. (1995). Conformational variability in the refined structure of the chaperonin GroEL at 2.8 Å resolution. Nat. Struct. Biol. *2*, 1083–1094.

Brunger, A.T., Adams, P.D., Clore, G.M., DeLano, W.L., Gros, P., Grosse-Kunstleve, R.W., Jiang, J.S., Kuszewski, J., Nilges, M., Pannu, N.S., et al. (1998). Crystallography & NMR system: a new software suite for macromolecular structure determination. Acta Crystallogr. D Biol. Crystallogr. *54*, 905–921.

Bukau, B., and Horwich, A.L. (1998). The Hsp70 and Hsp60 chaperone machines. Cell *92*, 351–366.

CCP4 (Collaborative Computational Project 4) (1994). The CCP4 suite: programs for protein crystallography. Acta Crystallogr. D Biol. Crystallogr. D *50*, 760–763.

Chen, L., and Sigler, P.B. (1999). The crystal structure of a GroEL/peptide complex: plasticity as a basis for substrate diversity. Cell *99*, 757–768.

Chen, H.S., Singh, S.S., and Perdew, G.H. (1997). The Ah receptor is a sensitive target of geldanamycin-induced protein turnover. Arch. Biochem. Biophys. *348*, 190–198.

Chothia, C. (1984). Principles that determine the structure of proteins. Annu. Rev. Biochem. *53*, 537–572.

Csermely, P., and Kahn, C.R. (1991). The 90-kDa heat shock protein (hsp-90) possesses an ATP binding site and autophosphorylating activity. J. Biol. Chem. *266*, 4943–4950.

de Carcer, G., do Carmo Avides, M., Lallena, M.J., Glover, D.M., and Gonzalez, C. (2001). Requirement of Hsp90 for centrosomal function reflects its regulation of Polo kinase stability. EMBO J. *20*, 2878–2884.

DeLano, W.L. (2002). The PyMOL Molecular Graphics System. http://www.pymol.org.

Dutta, R., and Inouye, M. (2000). GHKL, an emergent ATPase/kinase superfamily. Trends Biochem. Sci. *25*, 24–28.

Fontana, J., Fulton, D., Chen, Y., Fairchild, T.A., McCabe, T.J., Fujita, N., Tsuruo, T., and Sessa, W.C. (2002). Domain mapping studies reveal that the M domain of hsp90 serves as a molecular scaffold to regulate Akt-dependent phosphorylation of endothelial nitric oxide synthase and NO release. Circ. Res. *90*, 866–873.

Freeman, B.C., and Yamamoto, K.R. (2002). Disassembly of transcriptional regulatory complexes by molecular chaperones. Science *296*, 2232–2235.

Garnier, C., Lafitte, D., Jorgensen, T.J., Jensen, O.N., Briand, C., and Peyrot, V. (2001). Phosphorylation and oligomerization states of native pig brain HSP90 studied by mass spectrometry. Eur. J. Biochem. *268*, 2402–2407.

Hartson, S.D., Thulasiraman, V., Huang, W., Whitesell, L., and Matts, R.L. (1999). Molybdate inhibits hsp90, induces structural changes in its C-terminal domain, and alters its interactions with substrates. Biochemistry *38*, 3837–3849.

Hendrickson, W.A. (1991). Determination of macromolecular structures from anomalous diffraction of synchrotron radiation. Science *254*, 51–58.

Holm, L., and Sander, C. (1993). Protein structure comparison by alignment of distance matrices. J. Mol. Biol. *233*, 123–138.

Holton, J., and Alber, T. (2004). Automated protein crystal structure determination using ELVES. Proc. Natl. Acad. Sci. USA *101*, 1537–1542

Johnson, B.D., Chadli, A., Felts, S.J., Bouhouche, I., Catelli, M.G., and Toft, D.O. (2000). hsp90 chaperone activity requires the full-length protein and interaction among its multiple domains. J. Biol. Chem. *275*, 32499–32507.

Jones, T.A., Zou, J.Y., Cowan, S.W., and Kjeldgaard, M. (1991). Improved methods for binding protein models in electron density maps and the location of errors in these models. Acta Crystallogr. A *47*, 110–119.

Kampranis, S.C., Bates, A.D., and Maxwell, A. (1999). A model for the mechanism of strand passage by DNA gyrase. Proc. Natl. Acad. Sci. USA *96*, 8414–8419.

Kleywegt, G.J., and Jones, T.A. (1999). Software for handling macromolecular envelopes. Acta Crystallogr. D Biol. Crystallogr. *55*, 941–944.

Leslie, A.G.W. (1992). Recent changes to the MOSFLM package for processing film and image plate data. Joint CCP4+ESF-EAMCB Newsletter on Protein Crystallography, Number 26.

Louvion, J.F., Warth, R., and Picard, D. (1996). Two eukaryote-specific regions of Hsp82 are dispensable for its viability and signal

transduction functions in yeast. Proc. Natl. Acad. Sci. USA *93*, 13937–13942.

Marcu, M.G., Chadli, A., Bouhouche, I., Catelli, M., and Neckers, L.M. (2000). The heat shock protein 90 antagonist novobiocin interacts with a previously unrecognized ATP-binding domain in the carboxyl terminus of the chaperone. J. Biol. Chem. *275*, 37181–37186.

Meng, X., Devin, J., Sullivan, W.P., Toft, D., Baulieu, E.E., and Catelli, M.G. (1996). Mutational analysis of Hsp90 alpha dimerization and subcellular localization: dimer disruption does not impede "in vivo" interaction with estrogen receptor. J. Cell Sci. *109*, 1677–1687.

Meyer, P., Prodromou, C., Hu, B., Vaughan, C., Roe, S.M., Panaretou, B., Piper, P.W., and Pearl, L.H. (2003). Structural and functional analysis of the middle segment of hsp90. Implications for ATP hydrolysis and client protein and cochaperone interactions. Mol. Cell *11*, 647–658.

Meyer, P., Prodromou, C., Liao, C., Hu, B., Mark Roe, S., Vaughan, C.K., Vlasic, I., Panaretou, B., Piper, P.W., and Pearl, L.H. (2004). Structural basis for recruitment of the ATPase activator Aha1 to the Hsp90 chaperone machinery. EMBO J. *23*, 511–519.

Nathan, D.F., and Lindquist, S. (1995). Mutational analysis of Hsp90 function: interactions with a steroid receptor and a protein kinase. Mol. Cell. Biol. *15*, 3917–3925.

Neckers, L. (2002). Hsp90 inhibitors as novel cancer chemotherapeutic agents. Trends Mol. Med. *8*, S55–S61.

Nemoto, T., Ohara-Nemoto, Y., Ota, M., Takagi, T., and Yokoyama, K. (1995). Mechanism of dimer formation of the 90-kDa heat-shock protein. Eur. J. Biochem. *233*, 1–8.

Nemoto, T., Matsusaka, T., Ota, M., Takagi, T., Collinge, D.B., and Walther-Larsen, H. (1996). Dimerization characteristics of the 94-kDa glucose-regulated protein. J. Biochem. (Tokyo) *120*, 249–256.

Nemoto, T.K., Ono, T., Kobayakawa, T., Tanaka, E., Baba, T.T., Tanaka, K., Takagi, T., and Gotoh, T. (2001). Domain-domain interactions of HtpG, an Escherichia coli homologue of eukaryotic HSP90 molecular chaperone. Eur. J. Biochem. *268*, 5258–5269.

Otwinowski, Z., and Minor, W. (1997). Processing of X-ray diffraction data collected in oscillation mode. In Methods in Enzymology, C. Carter, W., Jr., and R.M. Sweet, eds. (San Diego, Academic Press), pp. 307–326.

Owen, B.A., Sullivan, W.P., Felts, S.J., and Toft, D.O. (2002). Regulation of heat shock protein 90 ATPase activity by sequences in the carboxyl terminus. J. Biol. Chem. *277*, 7086–7091.

Pratt, W.B., and Toft, D.O. (1997). Steroid receptor interactions with heat shock protein and immunophilin chaperones. Endocr. Rev. *18*, 306–360.

Prodromou, C., Roe, S.M., O'Brien, R., Ladbury, J.E., Piper, P.W., and Pearl, L.H. (1997). Identification and structural characterization of the ATP/ADP-binding site in the Hsp90 molecular chaperone. Cell *90*, 65–75.

Prodromou, C., Panaretou, B., Chohan, S., Siligardi, G., O'Brien, R., Ladbury, J.E., Roe, S.M., Piper, P.W., and Pearl, L.H. (2000). The ATPase cycle of Hsp90 drives a molecular "clamp" via transient dimerization of the N-terminal domains. EMBO J. *19*, 4383–4392.

Queitsch, C., Sangster, T.A., and Lindquist, S. (2002). Hsp90 as a capacitor of phenotypic variation. Nature *417*, 618–624.

Richter, K., Muschler, P., Hainzl, O., and Buchner, J. (2001). Coordinated ATP hydrolysis by the Hsp90 dimer. J. Biol. Chem. *276*, 33689–33696.

Riehl, R.M., Sullivan, W.P., Vroman, B.T., Bauer, V.J., Pearson, G.R., and Toft, D.O. (1985). Immunological evidence that the nonhormone binding component of avian steroid receptors exists in a wide range of tissues and species. Biochemistry *24*, 6586–6591.

Roe, S.M., Ali, M.M., Meyer, P., Vaughan, C.K., Panaretou, B., Piper, P.W., Prodromou, C., and Pearl, L.H. (2004). The mechanism of Hsp90 regulation by the protein kinase-specific cochaperone p50(cdc37). Cell *116*, 87–98.

Rutherford, S.L., and Lindquist, S. (1998). Hsp90 as a capacitor for morphological evolution. Nature *396*, 336–342.

Sato, S., Fujita, N., and Tsuruo, T. (2000). Modulation of Akt kinase activity by binding to Hsp90. Proc. Natl. Acad. Sci. USA *97*, 10832–10837.

Scheibel, T., Weikl, T., and Buchner, J. (1998). Two chaperone sites in Hsp90 differing in substrate specificity and ATP dependence. Proc. Natl. Acad. Sci. USA *95*, 1495–1499.

Scheufler, C., Brinker, A., Bourenkov, G., Pegoraro, S., Moroder, L., Bartunik, H., Hartl, F.U., and Moarefi, I. (2000). Structure of TPR domain-peptide complexes: critical elements in the assembly of the Hsp70-Hsp90 multichaperone machine. Cell *101*, 199–210.

Shaknovich, R., Shue, G., and Kohtz, D.S. (1992). Conformational activation of a basic helix-loop-helix protein (MyoD1) by the C-terminal region of murine HSP90 (HSP84). Mol. Cell. Biol. *12*, 5059–5068.

Shue, G., and Kohtz, D.S. (1994). Structural and functional aspects of basic helix-loop-helix protein folding by heat-shock protein 90. J. Biol. Chem. *269*, 2707–2711.

Soti, C., Racz, A., and Csermely, P. (2002). A Nucleotide-dependent molecular switch controls ATP binding at the C-terminal domain of Hsp90. N-terminal nucleotide binding unmasks a C-terminal binding pocket. J. Biol. Chem. *277*, 7066–7075.

Stebbins, C.E., Russo, A.A., Schneider, C., Rosen, N., Hartl, F.U., and Pavletich, N.P. (1997). Crystal structure of an Hsp90-geldanamycin complex: targeting of a protein chaperone by an antitumor agent. Cell *89*, 239–250.

Sullivan, W.P., and Toft, D.O. (1993). Mutational analysis of hsp90 binding to the progesterone receptor. J. Biol. Chem. *268*, 20373–20379.

Terwilliger, T.C., and Berendzen, J. (1999). Automated MAD and MIR structure solution. Acta Crystallogr. D Biol. Crystallogr. *55*, 849–861.

Walther, D. (1997). WebMol–a Java-based PDB viewer. Trends Biochem. Sci. *22*, 274–275.

Wegele, H., Muschler, P., Bunck, M., Reinstein, J., and Buchner, J. (2003). Dissection of the contribution of individual domains to the ATPase mechanism of Hsp90. J. Biol. Chem. *278*, 39303–39310.

Weikl, T., Muschler, P., Richter, K., Veit, T., Reinstein, J., and Buchner, J. (2000). C-terminal regions of Hsp90 are important for trapping the nucleotide during the ATPase cycle. J. Mol. Biol. *303*, 583–592.

Yamada, S., Ono, T., Mizuno, A., and Nemoto, T.K. (2003). A hydrophobic segment within the C-terminal domain is essential for both client-binding and dimer formation of the HSP90-family molecular chaperone. Eur. J. Biochem. *270*, 146–154.

Young, J.C., Schneider, C., and Hartl, F.U. (1997). In vitro evidence that hsp90 contains two independent chaperone sites. FEBS Lett. *418*, 139–143.

Young, J.C., Obermann, W.M., and Hartl, F.U. (1998). Specific binding of tetratricopeptide repeat proteins to the C-terminal 12-kDa domain of hsp90. J. Biol. Chem. *273*, 18007–18010.

Young, J.C., Hoogenraad, N.J., and Hartl, F.U. (2003). Molecular chaperones Hsp90 and Hsp70 deliver preproteins to the mitochondrial import receptor Tom70. Cell *112*, 41–50.

Accession Numbers

The experimental structure factors and coordinates of the refined model are deposited in the Protein Data Bank under code 1SF8.